Modeling Year-to-Year Variations of Clear-Sky Land Surface Temperature Using Aqua/MODIS Data

Zefeng Xing, Yanru Yu, Si-Bo Duan, Zhao-Liang Li, Maofang Gao, Pei Leng, Xia Zhang, Guofei Shang

▶ **To cite this version:**

Zefeng Xing, Yanru Yu, Si-Bo Duan, Zhao-Liang Li, Maofang Gao, et al.. Modeling Year-to-Year Variations of Clear-Sky Land Surface Temperature Using Aqua/MODIS Data. IEEE Access, 2020, 8, pp.114541-114553. 10.1109/ACCESS.2020.3003990 . hal-03005958

HAL Id: hal-03005958
https://hal.science/hal-03005958

Submitted on 23 Nov 2020

HAL is a multi-disciplinary open access archive for the deposit and dissemination of scientific research documents, whether they are published or not. The documents may come from teaching and research institutions in France or abroad, or from public or private research centers.

L'archive ouverte pluridisciplinaire **HAL**, est destinée au dépôt et à la diffusion de documents scientifiques de niveau recherche, publiés ou non, émanant des établissements d'enseignement et de recherche français ou étrangers, des laboratoires publics ou privés.

IEEE Access
Multidisciplinary | Rapid Review | Open Access Journal

Received May 29, 2020, accepted June 12, 2020, date of publication June 22, 2020, date of current version July 1, 2020.

Digital Object Identifier 10.1109/ACCESS.2020.3003990

Modeling Year-to-Year Variations of Clear-Sky Land Surface Temperature Using Aqua/MODIS Data

ZEFENG XING[1,2], YANRU YU[1], SI-BO DUAN[1], (Member, IEEE), ZHAO-LIANG LI[1,2], MAOFANG GAO[1], (Member, IEEE), PEI LENG[1], XIA ZHANG[3], AND GUOFEI SHANG[3]

[1]Key Laboratory of Agricultural Remote Sensing, Ministry of Agriculture/Institute of Agricultural Resources and Regional Planning, Chinese Academy of Agricultural Sciences, Beijing 100081, China
[2]ICube, UdS, CNRS, 67412 Illkirch, France
[3]School of Land Resources and Urban Rural Planning, Hebei GEO University, Shijiazhuang 050031, China

Corresponding authors: Zhao-Liang Li (lizhaoliang@caas.cn) and Guofei Shang (shangguofei@hgu.edu.cn)

This work was supported in part by the Fundamental Research Funds for Central Non-profit Scientific Institution under Grant 1610132019049. The work of Zefeng Xing was supported by the China Scholarship Council (CSC) under Grant 201800320098.

ABSTRACT Land surface temperature (LST) and its annual or inter-annual variations play an important role in understanding global climate change, urban heat island, and the process of land-atmosphere energy exchange. Many annual temperature cycle (ATC) models [i.e., ATC with three or five parameters (ACP3 or ACP5)] have been proposed to analyze the annual variations of LST in the past decades. In this study, two year-to-year continuous and derivable models (YYCD_ACP3 and YYCD_ACP5 models) were proposed to model several years of ATCs. The fitting results of the YYCD_ACP3 model with global Aqua/MODIS daytime LSTs from 2014 to 2018 show that the YYCD_ACP3 model achieved a good performance in fitting the time-series LSTs with an overall normalized root-mean-square error (NRMSE) of 0.21, coefficient of determination (R^2) of 0.74, and refined index of agreement (d) of 0.85. In addition, the modeling results of ten representative samples covering different climatic conditions and land cover worldwide show that, except for two sites located in tropical and Antarctic, the YYCD_ACP3 model could show a good performance with R^2 greater than 0.6. Although the ACP3 model shows similar performance to the YYCD_ACP3 model, the fitting curve of the YYCD_ACP3 model is continuous and smooth for describing the interannual variations of LST. When the LSTs of 2014–2018 are fitted as a whole by using both models, the YYCD_ACP3 model shows a slightly better performance than that of the ACP3 model. The application of the YYCD_ACP3 model with the global MODIS LSTs from 2003 to 2018 indicates that the results of the YYCD_ACP3 model have the potential to reveal the interannual variations of LST. Therefore, we conclude that the YYCD models are valuable for modeling the variations of LST over several years and can be widely applied.

INDEX TERMS Land surface temperature, annual temperature cycle, modeling, MODIS.

I. INTRODUCTION

Land surface temperature (LST), which is measured using a remote sensor from the ground or space to represent the radiative skin temperature of the land surface, is one of the most important parameters in global and regional processes of surface energy and water balance [1]–[3]. It is widely used in various applications, for example, accurate knowledge of LST can provide important information on climate change, hydrological cycle, vegetation monitoring, and urban heat island studies [4]–[7]. However, LST is a physical quantity that changes in both time and space owing to the variations in solar radiation, land use/cover changes, and also changes in climate. Compared with conventional ground single-point measurements, satellite-based remote sensing can measure the LST continuously over time worldwide with sufficiently high temporal resolution.

Over the past decades, a number of temporal models have been built to describe the variations of LST over time; these include the diurnal temperature cycle (DTC) models and annual temperature cycle (ATC) models [8]–[10]. The DTC models describe the variations of LST over a short period

The associate editor coordinating the review of this manuscript and approving it for publication was Yue Zhang.

This work is licensed under a Creative Commons Attribution 4.0 License. For more information, see https://creativecommons.org/licenses/by/4.0/

(one day or several days). Notably, the DTC models can only fit the LST data of almost complete cloud-free days, thus limiting their promotion and application [11]. In contrast, the ATC models usually describe the seasonal or interannual variations of LST. The parameters in the ATC model are closely related to the physical properties of the land surface [12], [13]. For example, the annual mean surface temperature and annual amplitude are important parameters in urbanization studies and urban heat island analysis [14]–[16]. The phase shifts from the start day in the annual cycle are related to changes in climate [17]. For instance, some studies have shown that phase shifts in the annual temperature cycle during the past decades are related to atmospheric CO_2 concentrations [18], [19]. These parameters can also be used as disaggregation kernels for downscaling LST to enhance its spatial resolution [20], [21]. Compared with other methods that combine multiple surface parameters to downscaling land surface temperatures [22], [23], the ATC model method is simpler because it does not require the participation of other surface parameters, such as land cover types and vegetation index. In addition, the ATC models can be used to produce spatiotemporal continuous LSTs [24]. Therefore, modeling the annual LST cycle is very important for many research fields.

The currently available ATC models can be divided into two groups. The first group uses a constant term plus a trigonometric function (i.e., the ACP3 and ACP5 models) to fit LST dynamics for an annual cycle. For instance, Bechtel (2011) used a simple sine function to model one-year LSTs of clear-sky for one pixel at the same time of each day [8]. After that, a new model with two sine functions was suggested to model tropical scenarios, where the performance could be improved [25]. These two models are simple and have a robust physical basis [26]. Later, some researchers proposed a hybrid framework with the related surface parameters, such as air temperature, soil moisture, albedo, and the relative humidity for modeling the annual dynamics of satellite-derived LST [27], [28]. Although this framework can achieve higher accuracy, it is complicated because of the input of a large amount of auxiliary data. The second group of ATC models uses a decomposition model to analyze landscape thermal patterns for multiple years. The first group of models can only capture the averaged LST variation for one year, and ignore gradual or abrupt changes over several years. Therefore, Fu and Weng (2015) and Quan *et al.* (2016) proposed a decomposition model with different parameters to deal with the unevenly distributed time-series data to understand both the annual and inter-annual LST variations [29], [30]. In these decomposition models, the remotely sensed LST time series can be decomposed into the trend, seasonal, and noise components. Although the decomposition model can achieve the annual mean surface temperature trends, it cannot obtain the annual amplitude and annual phase trends, which are very important for related research. Therefore, such a model cannot capture the detailed variations of LST for specific years. Moreover, if we use the first group models, i.e., the ACP3 or ACP5 models to simulate the LST data for each year, the fitting curve of the adjacent years is discontinuous with respect to time. Ideally, the fitted curve of LST changes over several years should be continuous and smooth with time. Therefore, a new ATC model is needed to describe the inter-annual variations of LST.

In view of the fact that the current ATC models are usually used to fit the LST change in a single year, in order to increase the adaptability of the ATC models to fit the LST change for several years, the objective of this study is to develop a year-to-year continuous and derivable model for modeling the inter-annual variations of LST from MODIS data. In this paper, the authors propose year-to-year continuous and derivable ATC models (YYCD) based on ACP3 and ACP5 to model the LST variations over several years. The paper is organized as follows. Section 2 presents the ACP3, ACP5, and YYCD models. Section 3 introduces the data used in this study. In Section 4, we present and discuss the fitting results of the ATC models. Finally, the conclusions are derived in Section 5.

II. METHODOLOGY

The ACP3 and ACP5 models are usually used for modeling the variations of LST for a single year. In this section, the ACP3 and ACP5 models are introduced first. Then, the YYCD_ACP3 and YYCD_ACP5 models are derived by taking into account the physical continuity and derivability of LST between the adjacent years. Finally, we introduced three indicator formulas for model evaluation.

A. ACP3 MODEL

Bechtel (2011) proposed a simple ATC model with three annual cycle parameters (ACP3) to fit the variations of LST for long time-series [8]. The model consists of a constant and a sine function with the reference day of the spring equinox. To better explain the physical meaning of the phase in the model, we used the cosine function instead of the sine function in this study and the reference day is the first day of the year:

$$LST(t) = a + b\cos\left[\frac{2\pi}{\omega}(t-c)\right] \tag{1}$$

where LST is the cloud-free LST at the same time each day, t is the day of the year, a is the annual mean surface temperature, b is the annual amplitude of the surface temperature, c is the phase, that is, the day when LST reaches its maximum values of the year, and ω is the annual cycle, which is 365 in common years and 366 in leap years.

B. ACP5 MODEL

Based on the ACP3 model, Bechtel (2018) suggested an alternative ATC model with five parameters (referred as ACP5) to improve the performance of the fit in the tropical areas [25]. The model is formulated as follows:

$$LST(t) = a + b_1\cos\left[\frac{2\pi}{\omega}(t-c_1)\right] + b_2\cos\left[\frac{4\pi}{\omega}(t-c_2)\right] \tag{2}$$

where a is the annual mean surface temperature, b_1 and b_2 are the amplitudes of the annual and biannual variations, respectively; and c_1 and c_2 are the respective phases.

C. YYCD MODEL

The aforementioned ACP3 and ACP5 models are generally used to describe the seasonal variation of LST for a single year. Here, we show the use of ACP3 and ACP5 models to model the annual temperature cycles for several years. Considering the physical continuity and derivability of LST variations over several years, the fitting curve of the LST variations for adjacent years is assumed to be continuous and derivable. According to Eq. (1), the variations of LST for the year i and $i+1$ can be expressed as:

$$LST^i(t) = a^i + b^i \cos[\frac{2\pi}{\omega}(t - c^i)] \tag{3}$$

$$LST^{i+1}(t) = a^{i+1} + b^{i+1} \cos[\frac{2\pi}{\omega}(t - c^{i+1})] \tag{4}$$

where t represents a day of several years and $t \in [365(i-1) + k_i + 1, 365i + k_{i+1}]$ for year i (Eq. (3)), and k_i is the number of leap years before year i.

To make the fitting curve of the year i and $i+1$ continuous and derivable, we need to determine the junction point of the two fitted curves first. Here, we assume that the fitted curve is continuous and derivable at the midpoint ($t = t_m = 365i + k_{i+1} + 0.5$) between the last day of the year i and the first day of year $i+1$. Thus, the following two equations can be obtained at the point:

$$LST^i(t)|_{t=t_m} = LST^{i+1}(t)|_{t=t_m} \tag{5}$$

$$(\partial LST^i/\partial t)|_{t=t_m} = (\partial LST^{i+1}/\partial t)|_{t=t_m} \tag{6}$$

Then, we get

$$a^{i+1} = a^i + b^i \cos[\frac{2\pi}{\omega}(t_m - c^i)] - b^{i+1} \cos[\frac{2\pi}{\omega}(t_m - c^{i+1})] \tag{7}$$

$$b^{i+1} = b^i \sin[\frac{2\pi}{\omega}(t_m - c^i)] / \sin[\frac{2\pi}{\omega}(t_m - c^{i+1})] \tag{8}$$

By combining Eqs. (3), (4), (7), and (8), the year-to-year continuous and derivable model can be derived from the ACP3 (YYCD_ACP3) of LST variations. Eqs. (7) and (8) are the two constraints that ensure that the fitting curves of adjacent years are continuous and derivable. The total number of free parameters in the YYCD_ACP3 model for n ($n \geq 2$) years is $n+2$: a and b in the first year and c for each year. In addition, a and b for each year after the first year can be calculated using Eqs. (7) and (8).

Considering that the ACP3 model does not perform well in some cases [25], it is necessary to derive the corresponding YYCD model based on the ACP5 model. Thus, we can achieve the YYCD_ACP5 model through the following four equations:

$$LST^i(t) = a^i + b_1^i \cos[\frac{2\pi}{\omega}(t - c_1^i)] + b_2^i \cos[\frac{4\pi}{\omega}(t - c_2^i)] \tag{9}$$

TABLE 1. Initial values of the free parameters in the YYCD_ACP3 and YYCD_ACP5 models.

Parameters	YYCD_ACP3	YYCD_ACP5
a	T_{mean}	T_{mean}
b_1	$0.5\times(T_{max} - T_{min})$	$0.5\times(T_{max} - T_{min})$
c_1	180 for Northern Hemisphere and 360 for Southern Hemisphere	180 for Northern Hemisphere and 360 for Southern Hemisphere
b_2	-	$0.1\times(T_{max} - T_{min})$
c_2	-	90

T_{mean} is the mean LST of the year, and T_{max} and T_{min} represent the maximum and minimum LSTs of each year, respectively.

$$LST^{n+1}(t) = a^{i+1} + b_1^{i+1} \cos[\frac{2\pi}{\omega}(t - c_1^{i+1})] + b_2^{i+1} \cos[\frac{4\pi}{\omega}(t - c_2^{i+1})] \tag{10}$$

$$a^{i+1} = a^i + b^i \cos[\frac{2\pi}{\omega}(t_m - c_1^i)] + b_2^i \cos[\frac{4\pi}{\omega}(t_m - c_2^i)] - b_1^{i+1} \cos[\frac{4\pi}{\omega}(t_m - c_1^{i+1})] - b_2^{i+1} \cos[\frac{4\pi}{\omega}(t_m - c_2^{i+1})] \tag{11}$$

$$b_1^{i+1} = \frac{b_1^i \sin[\frac{4\pi}{\omega}(t_m - c_1^i)] + 2b_2^{i+1} \sin[\frac{4\pi}{\omega}(t_m - c_2^{i+1})]}{\sin[\frac{2\pi}{\omega}(t_m - c_1^{i+1})]} \tag{12}$$

Similarly, the total number of free parameters in the YYCD_ACP5 model for n ($n \geq 2$) years is $3n+2$ (i.e., a and b_1 in the first year and c_1, b_2, and c_2 for each year). Except for the first year, the values of a and b_1 are calculated through Eqs. (11) and (12).

As the YYCD_ACP3 and YYCD_ACP5 models are nonlinear models, the Powell optimization method proposed by Seiler (1989) was used to solve their free parameters [31]. The initial values of the free parameters are listed in Table 1. The closer the initial value is to the final value, the faster is the model calculation speed.

D. MODEL EVALUATION

The modeling results were evaluated by normalized root-mean-square error (NRMSE), coefficient of determination (R^2), and refined index of agreement (d, [32]), which are commonly used as measurable indicators for fitting problems. The expressions are given as follows:

$$NRMSE = \frac{\sqrt{\frac{1}{n}\sum_{i=1}^{n}(LST_p - LST_o)^2}}{IQR} \tag{13}$$

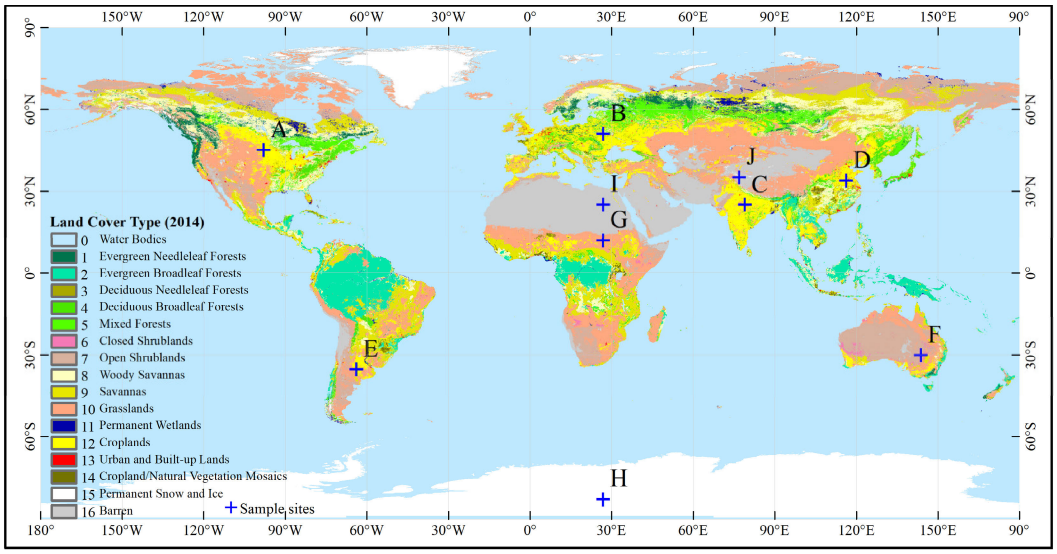

FIGURE 1. Land-cover types throughout the world obtained from the MODIS product MCD11C1 in 2014. The blue crosses represent the selected sample sites.

$$R^2 = 1 - \frac{\sum_{i=1}^{n} (LST_p - LST_o)^2}{\sum_{i=1}^{n} (LST_p - \overline{LST_o})^2} \tag{14}$$

$$d = \begin{cases} 1 - \dfrac{\sum_{i=1}^{n} \left|LST_p - LST_o\right|}{2\sum_{i=1}^{n} \left|LST_o - \overline{LST_o}\right|}, & when \\ \sum_{i=1}^{n} \left|LST_p - LST_o\right| \\ \leq 2\sum_{i=1}^{n} \left|LST_o - \overline{LST_o}\right| \\ \dfrac{2\sum_{i=1}^{n} \left|LST_o - \overline{LST_o}\right|}{\sum_{i=1}^{n} \left|LST_p - LST_o\right|} - 1, & when \\ \sum_{i=1}^{n} \left|LST_p - LST_o\right| \\ > 2\sum_{i=1}^{n} \left|LST_o - \overline{LST_o}\right| \end{cases} \tag{15}$$

where LST_p refers to the predicated LST from the ATC model, LST_o represents the observed MODIS LSTs, $\overline{LST_o}$ is the mean value of the observed LST in the time series, IQR is the interquartile range ($IQR = Q_3 - Q_1$, with $Q_1 = CDF^{-1}(0.25)$ and $Q_3 = CDF^{-1}(0.75)$, where CDF^{-1} is the quantile function), and n represents the total number of samples involved in the modeling. The reason we chose IQR to normalize RMSE is that there are outliers and extreme values in the LST series.

III. DATA

Satellite data obtained from the Moderate Resolution Imaging Spectroradiometer (MODIS) daily LST product MYD11C1 Version 6 (onboard Aqua satellite) were used in this study. This MODIS product can be acquired from the NASA Earth Science Data (https://search.earthdata.nasa.gov) and is directly derived from the MYD11B1 product. The MYD11C1 product is generated through a physics-based day/night algorithm and it provides daily LST and land surface emissivity (LSE) values at 0.05° (5600 m for the equator) latitude/longitude climate modeling grid (CMG) [33]. The CMG cells follow a geographic grid with 7200 columns and 3600 rows, representing the entire Earth.

The daytime LSTs (about 1:30 pm) from 2014 to 2018 were used to evaluate the YYCD model. The MODIS LSTs used in this study were filtered through its quality assurance (QA) file to ensure the average LST error is less than 2.0 °. In addition, in order to further display the fitting results of the ATC models, ten representative locations were selected, each with different land covers. The detailed information of the selected sites is shown in Table 2.

IV. RESULTS AND DISCUSSION

A. ACCURACY ASSESSMENTS OF THE YYCD_ACP3 MODEL

The performance of the YYCD_ACP3 model was evaluated using the Aqua/MODIS daytime LSTs from January 1, 2014, to December 31, 2018. Figure 2(a)–2(j) illustrates the fitting result of the YYCD_ACP3 (red curve) and ACP3 models (blue curve) for five years at ten representative samples (sites A–J). This selected five-year period is taken as an example of continuous and derivable years of time.

The NRMSE of the YYCD_ACP3 model at the ten sites are 0.43, 0.37, 0.43, 0.30, 0.35, 0.25, 0.80, 0.29, 0.25, and 0.38, respectively. Lower NRMSE values indicate less residual variance. The R^2 values of the YYCD_ACP3 model are

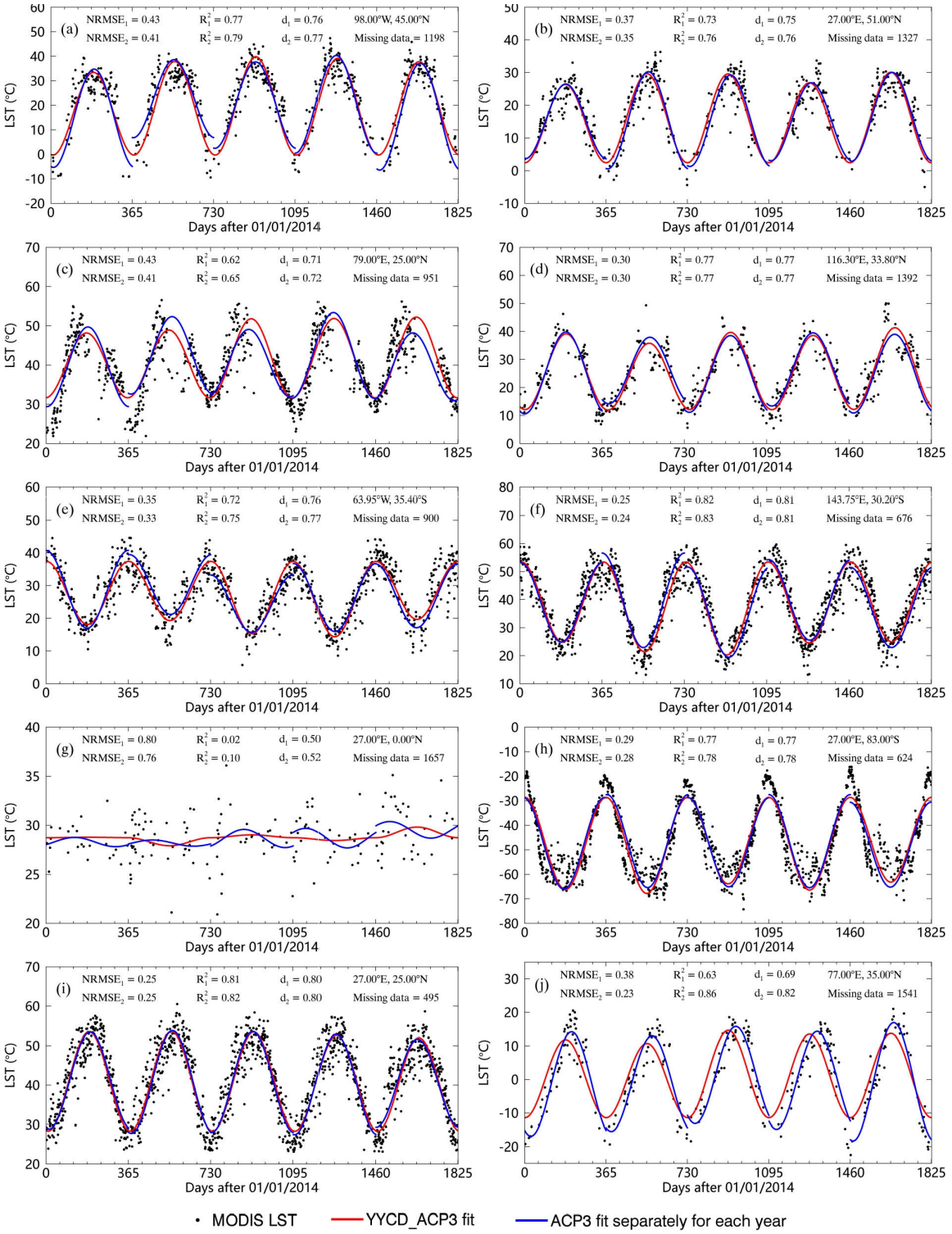

FIGURE 2. YYCD_ACP3 model fitting Aqua/MODIS daytime LSTs from 2014 to 2018 at sites A–J and ACP3 model fitting the LSTs independently for each year. The red and blue curves are the fitting results of the YYCD_ACP3 and ACP3 models, respectively. The subscripts 1 and 2 of NRMSE, R^2, and *d* represent the YYCD_ACP3 model and the ACP3 model, respectively.

greater than 0.6 except for site G at the equator with a value of 0.02. In terms of *d*, except for site G with *d* of 0.50, the *d* values of all other sites are greater than 0.70. Overall, the fitting results indicate that the YYCD_ACP3 model shows good performance to fit the MODIS LSTs at site A, B, D, E, F, I and J. However, these sites located tropical (i.e. site C and G)

TABLE 2. Description of the selected samples.

Site ID	Longitude	Latitude	Elevation	Land cover type
A	98.00° W	45.00° N	1455 m	Grassland
B	27.00° E	51.00° N	195 m	Mixed Forests
C	79.00° E	25.00° N	283 m	Cropland
D	116.30° E	33.80° N	32 m	Cropland
E	63.95° W	35.40° S	147 m	Cropland
F	143.75° W	30.20° S	155 m	Savanna
G	27.00° E	0.00° N	753 m	Broadleaf Forest
H	27.00° E	83.00° S	2840 m	Permanent ice
I	27.00° E	25.00° N	538 m	Barren
J	77.00° E	35.00° N	5255 m	Permanent ice

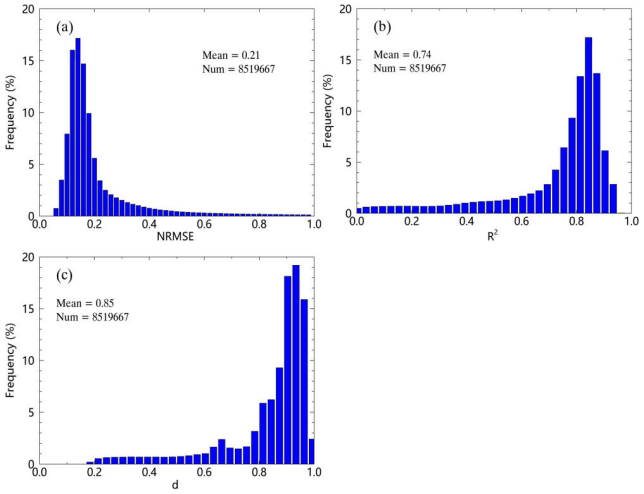

FIGURE 3. Histogram of the (a) NRMSE, (b) R^2, and (c) *d* of the YYCD_ACP3 model for fitting global MODIS LSTs from 2014 to 2018.

and cold regions (i.e. site H) show a different variation of LST with R^2 of lower than 0.7. As can be seen in Figure 2(c), 2(h), the YYCD_ACP3 model does not describe well the annual variations of LST at site C and site H. For site C (79°E, 25°N), which is located in tropical zone, LST shows a decreasing trend due to the cooling effect of the high coverage vegetation in the rainy season and LST will be increasing rapidly because of the harvest of farmland, where the fractional vegetation cover drops rapidly in a short time. For site G (Figure 2(g)), which is located at the equator, the annual amplitude throughout the year is very small because the solar radiation changes little throughout the year. For station H located in Antarctica, the YYCD_ACP3 model performs poorly in describing the variation of LST during the polar days. The reason for this is that the phenomenon of polar day/night. The sunrise and sunset dates for site E are October 5 and March 7, respectively (https://www.esrl.noaa.gov/gmd/grad/solcalc/sunrise.html). During the polar nights (from March 7 to October 5),

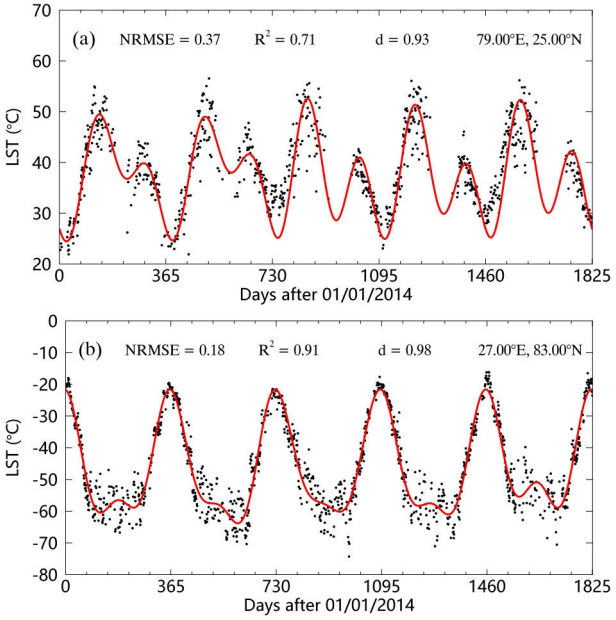

FIGURE 4. YYCD_ACP5 model fitting Aqua/MODIS daytime LSTs from 2014 to 2018 at site C (a) and site H (b).

LST fluctuates less because there is no solar radiation. However, LST increases as the sun's altitude increases during the polar days. For these sites located in tropical and polar, we can use the YYCD_ACP5 model with more free parameters to simulate the inter-annual variation of LST. As shown in Figure 4(a) and 4(b), the YYCD_ACP5 model performs better than the YYCD_ACP3 model at site C and site H (i.e. Figure 2(c) and 2(h)) with NRMSE of 0.37 and 0.18, respectively and R^2 of 0.71 and 0.91, respectively. Compared with the YYCD_ACP3 model, the YYCD_ACP5 model can significantly improve the fitting accuracy in terms of NRMSE and R^2 values at site C and site H. Therefore, it is recommended to use the YYCD_ACP5 model to simulate the inter-annual variations of LST in the tropical and polar regions.

We also used the YYCD_ACP3 model to fit the annual variation of global MODIS daytime LSTs. Figure 3 shows the histograms of NRMSE, R^2, and *d* of the YYCD_ACP3 model for fitting global MODIS LSTs from 2014 to 2018. As can be seen in Figure 3, the range of NRMSE values is mostly less than 0.4 with a mean value of 0.21. In terms of R^2, the R^2 values are mostly great than 0.5 with a mean value of 0.74. And most *d* values are greater than 0.6 with a mean value of 0.85. The results indicate that the YYCD_ACP3 model can be widely applied to simulate the global annual variations of LST, although it performs poorly in a few locations, such as points in the tropics.

Compared with the ACP3 model, which fits the interannual variations of LST separately for each year, the NRMSE, R^2, and *d* values are approximately equal to that of the YYCD_ACP3 model. These results indicate that the YYCD_ACP3 model shows a similar performance with the ACP3 model. However, the fitting curve of the YYCD_ACP3 model is continuous and smooth

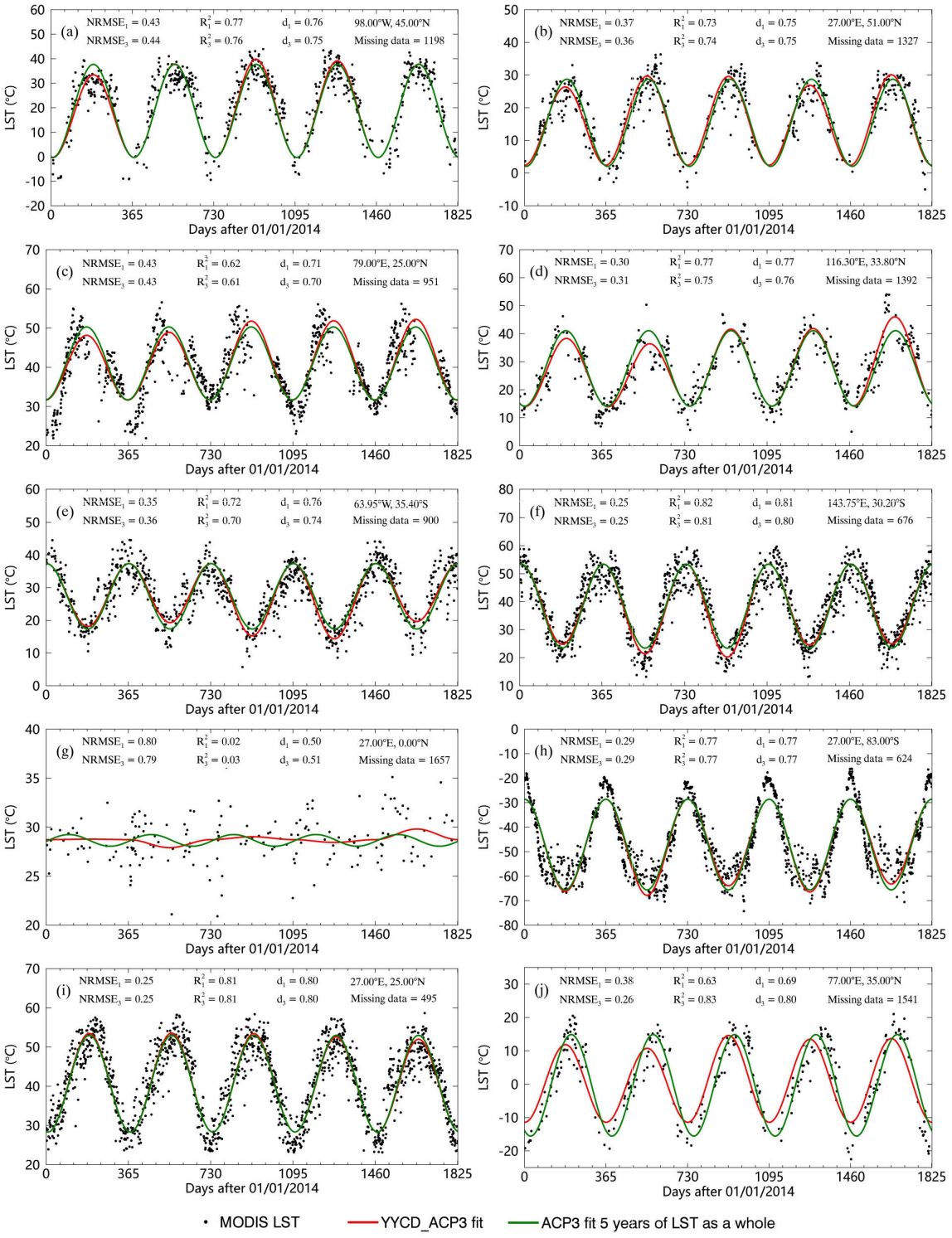

FIGURE 5. YYCD_ACP3 and ACP3 models fitting Aqua/MODIS daytime LSTs from 2014 to 2018 at site A–J. The red and green curves show the fitting results of the YYCD_ACP3 and ACP3 models, respectively.

for fitting the inter-annual variation of LST. As shown in Figure 2(a)–2(j), the fitting curve of the ACP3 model is physically segmented around the adjacent years, while the results of the YYCD_ACP3 model are not. The discontinuity of the fitted curves between years was resolved. This is because the ACP3 model fits each year's LST changes separately without considering the temporal progression of the inter-annual variation of LST. The fitting of the LST

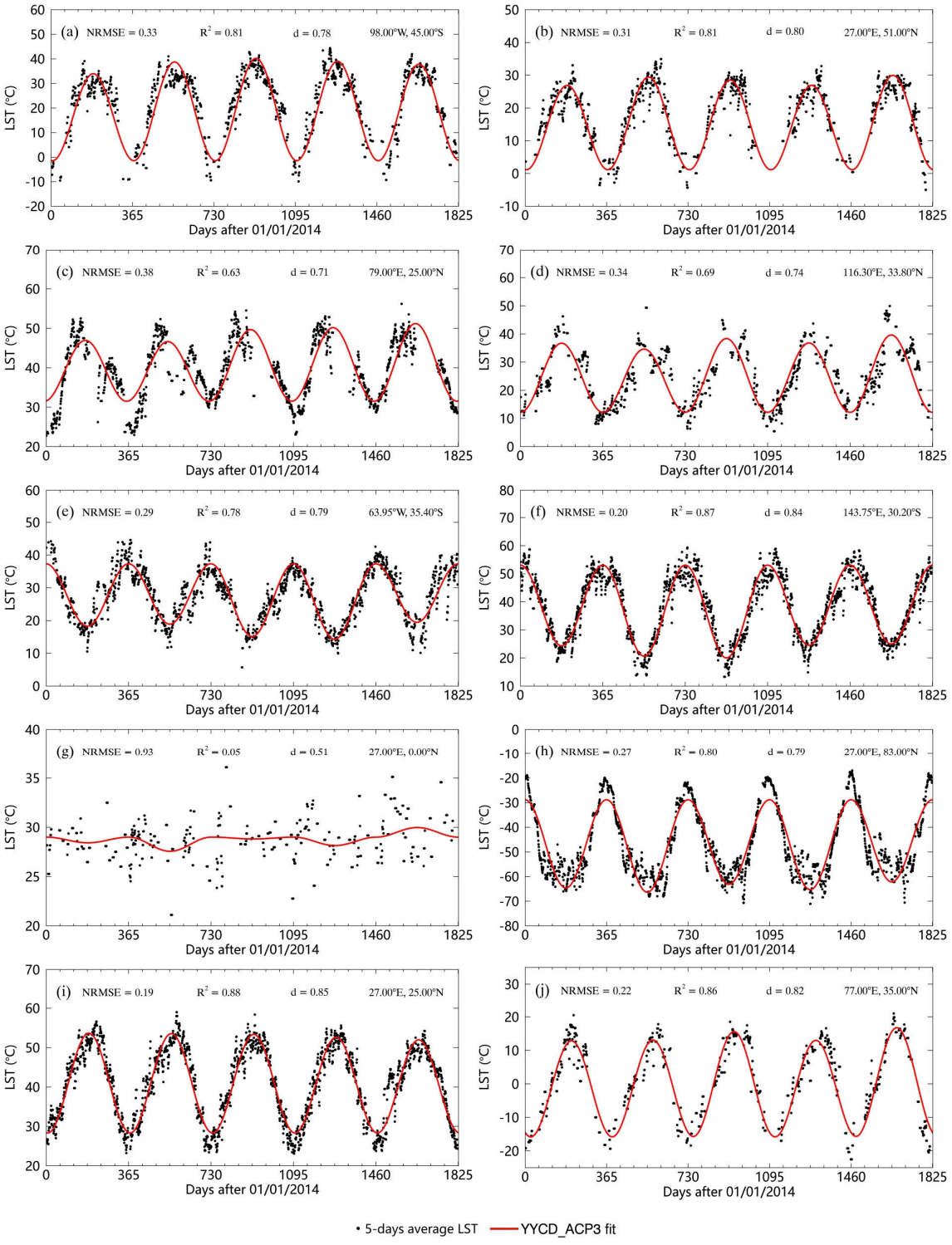

FIGURE 6. YYCD_ACP3 model fitting MODIS 5-days moving average LST data from 2014 to 2018 at site A–J. The red curve shows the fitting results of the YYCD_ACP3 model.

variations over several years into the YYCD_ACP3 model describes the continuous thermal conditions of land surface for many years and generates representative and informative ACPs [25]. The YYCD_ACP3 model could be beneficial to the analysis of inter-annual changes in ACPs. These ACPs depend on daily LSTs and are not influenced by some gaps due to cloud contamination [12]. These informative parameters can be used to study the LST climatology [12], [16] or to downscale LST images [27].

B. COMPARISON OF YYCD_ACP3 AND ACP3 MODELS

According to some previous studies, the ACP3 model can be used to model the inter-annual variation of LST [16], [25], and an important assumption being that the LST data series are cyclic-stationary over several years. Thus, the ACPs calculated from the ACP3 model fitting of the time–series LSTs reflect the average status over the years. However, the real changes of the LSTs over the years may not be the same sine or cosine function. For instance, the urbanization process, occurrence of wildfire, or climate changes over the years may affect the variation of LST. Figure 5(a)–(j) shows the fitting results of the YYCD_ACP3 and ACP3 models for modeling the variations of the LSTs from 2014 to 2018 at sites A–J. It is worth noting that the ACP3 model fits the five years of LST as a whole. The results show that the fitting curves of both the YYCD_ACP3 and ACP3 models are continuous and smooth over the five years. However, the YYCD_ACP3 model shows a slightly better performance than the ACP3 model at the six sites in terms of the NRMSE values. The NRMSE values of the YYCD_ACP3 model at sites A–J are 0.43, 0.37, 0.43, 0.30, 0.35, 0.25, 0.80, 0.29, 0.25, and 0.38, respectively, whereas those of the ACP3 model are 0.44, 0.36, 0.43, 0.31, 0.36, 0.25, 0.79, 0.29, 0.25, and 0.26, respectively. This difference in the results is mainly due to the YYCD_ACP3 model having more free parameters than the ACP3 model for modeling the five years of LST. The YYCD_ACP3 model comprises nine free parameters, whereas the ACP3 model has only three free parameters. The YYCD_ACP3 model can reflect the LST variation in each year, while the ACP3 model can only reflect an average LST variation for these five years. Taking site A as an example, the YYCD_ACP3 model can describe the detailed variations in the LSTs for each year, while the ACP3 model significantly overestimates the actual LST when the LST was highest in the first year. If the LSTs are cyclic-stationary over the five years, such as at site C, the two models perform similarly. Therefore, the YYCD_ACP3 model is suitable for analyzing the inter-annual variations in the LSTs.

C. APPLY THE YYCD_ACP3 MODEL WITH 5-DAYS MOVING DATA

Here, we applied the YYCD_ACP3 model with 5-days moving average LST data at site A-J. Figure 6(a)-(j) shows the fitting results of the YYCD_ACP3 model using the 5-days moving average LSTs from 2014 to 2018 at site A-J. Compare with the YYCD_ACP3 model fit the raw LST data, the NRMSE values at site A, B, C, E, F, H, I and J decreased by 0.10, 0.06, 0.05, 0.06, 0.05, 0.02, 0.06, and 0.16 respectively. However, its values at site D and G increase by 0.04 and 0.13 respectively. In terms of R^2, the value of site A, B, C, E, F, G, H, I, and J has increased and it decreases at site D. For the indicator d, the value of the two does not change much. These results show that using the YYCD_ACP3 model to fit the 5-days moving LST data can improve the fitting accuracy for some sites. The reason may be that after taking the average, the LST variability of the time series becomes smaller. But for some other sites, it will slightly reduce the fitting accuracy. The reason may be related to the uneven distribution of valid LST data in the time series.

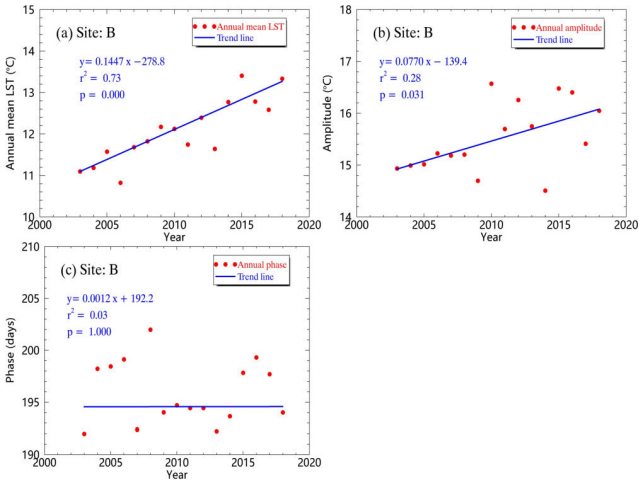

FIGURE 7. Trends of the (a) annual mean LST, (b) amplitude and (c) phase of the YYCD_ACP3 model from 2003 to 2018 at site B. The blue straight line is the trend line.

D. AN EXAMPLE APPLICATION OF THE YYCD_ACP3 MODEL

The YYCD models can be applied to observe the changes in the annual mean LST, amplitude, and phase for several years. Here, we used the YYCD_ACP3 model to fit the MODIS/Aqua daytime LSTs from 2003 to 2018 to produce ACPs. Then, we used the widely used Theil–Sen linear regression [34] and the Mann–Kendall (MK) test [35]–[37] for predicting the trends and performing a significance test of the three ACPs. Figure 7(a)–(c) show the trends of the annual mean LST, amplitude, and phase from 2003 to 2018 at site B based on the YYCD_ACP3 model. The annual mean LST and amplitude at site B show a significantly positive trend from 2003 to 2018 for the Theil-Sen slope of 0.1447 and 0.0770 °/year, respectively, and their corresponding P values are 0.000 and 0.031. According to land cover types at site B from 2003 to 2018, the site's land cover type has always been mixed forest and has not changed. Therefore, the reason for the apparent increase in the annual average LST and amplitude at this site may be related to global warming. However, the annual phase at site B does not show significant changes with the Theil–Sen slope of 0.0012 days/year and P-value of 1.000. A previous study showed that the changes in the annual phase were mainly related to the natural variability, such as the changes in phenology of vegetation or the changes in land cover types [17]. Therefore, a possible reason why the phase of station B has no obvious change trend is that the land cover type has not changed over the study period. The specific reason needs to further check the phenological change information of vegetation in this area.

We also used the proposed YYCD_ACP3 model to calculate the ACPs globally from 2003 to 2018 with MODIS

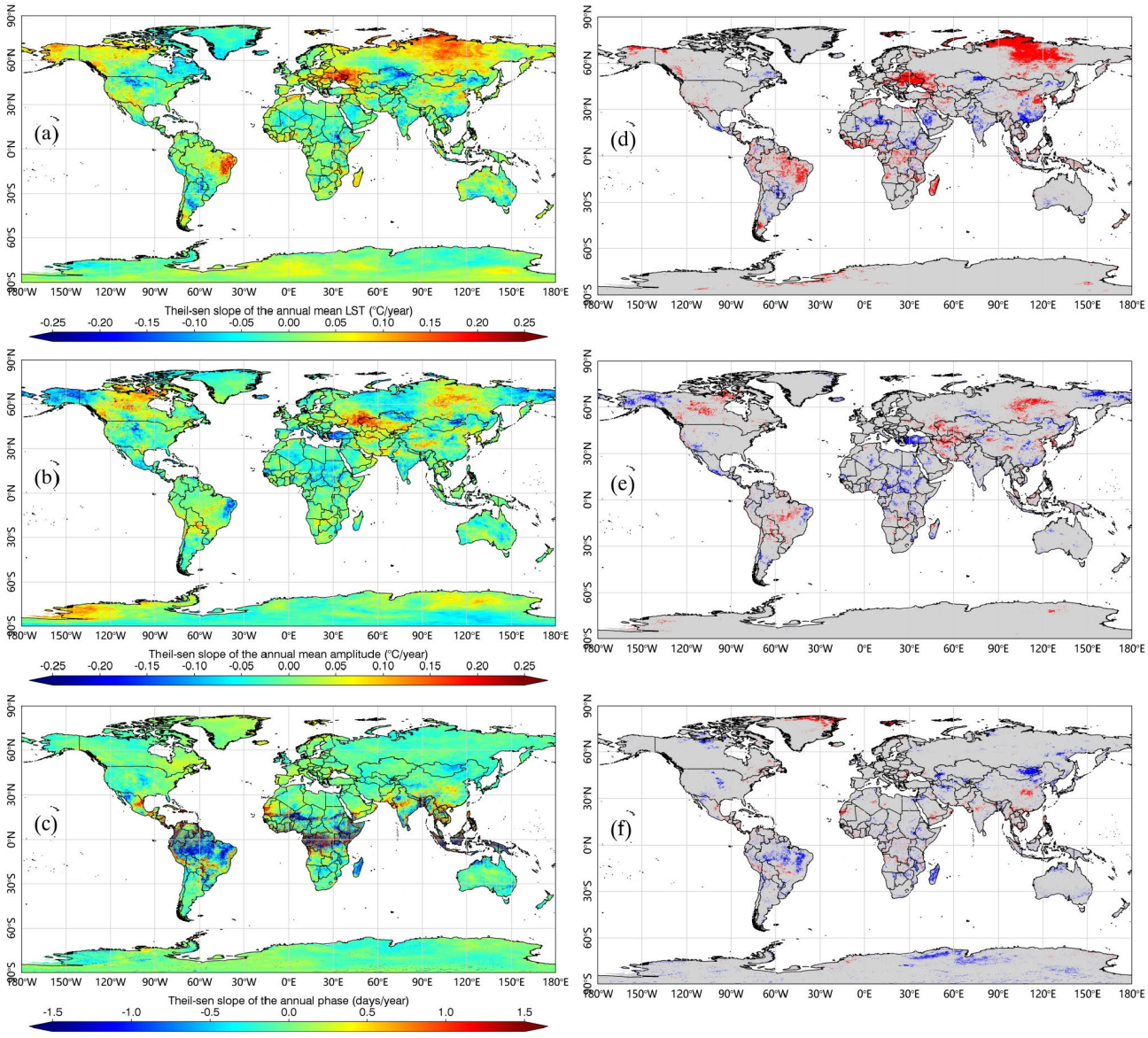

FIGURE 8. Global trends and MK test results of the annual mean LST, amplitude, and phase of the YYCD_ACP3 model from 2003 to 2018, (a), (b) and (c) are the Theil-Sen slope, respectively, (d), (e) and (f) are the corresponding MK test results, respectively (red: significant increase ($p<0.05$); blue: significant decrease ($p<0.05$); gray: no significant changes ($p \geq 0.05$)).

LSTs as the input. Figure 8(a)–(f) shows the global trends and MK test results of the annual mean LST, amplitude, and phase of the YYCD_ACP3 model from 2003 to 2018. Regarding the annual mean LST, the regions that are obviously warming are mainly distributed in eastern Brazil (4–19°S, 35–46°W), eastern Europe (44–54°N, 20–50°E), and north-central Russia (52°–77°N, 85–128°E). In contrast, the areas that became significantly colder are mainly distributed in Central Asia (43–58 °N, 60–82°E) and northern United States (39–53°N, 93–114°W). As previously reported, changes in precipitation, vegetation, land cover types, and global warming trends may be the causes of climate warming or cooling in these areas [38]. For example, Francini-Filho's research shows that the destruction of vegetation and reduced rainfall in eastern Brazil have led to warming of the region [39]. However, for high latitude areas, such as northern Russia, the increase in temperature will promote the growth of vegetation [40]. In terms of the annual amplitude, the regions showing a significant increase are mainly distributed in northern Canada (55–72° N, 86–121°W), western Asia (34–56°N, 35–65°E) and north-central Russia (51–70°N, 94–130°E). While the regions with significantly reduced of the annual amplitude are mainly distributed in Central Asia (48–56°N, 64–82°W) and the northern United States (36– 51°N, 98–110°W). For the global annual phase of the YYCD_ACP3 model, the areas with large significant changes are mainly located in Central Brazil (3–23°S, 40–60°W), Central Mongolia (42–50°N, 102–118°E), Central China

(32–35°N, 103–115°E). According to Stine's research, the changes in the annual phase were mainly related to the natural variability, such as the changes in phenology of vegetation or the changes in land cover type [17]. Therefore, the specific reason needs to further check the phenological change information of vegetation in these areas. However, we need to comprehensively consider the changes of these several parameters. Overall, the causes of these trends are poorly understood, and thus further analysis is required. For example, we should consider the impact of other variables such as land use type, vegetation, relative humidity and solar radiation on the surface temperature. In addition, because the study is relatively short, adding LST data from other sensors (such as Advanced Very High-Resolution Radiometer, AVHRR) to increase the LST of a longer time–series will help analyze the long-term sequence changes of LST.

E. LIMITATIONS

In this paper, the proposed YYCD_ACP3 model performs well in analyzing the inter-annual variation of LST. However, the YYCD_ACP3 model comprises several limitations that require attention in the future. First, the data used in the YYCD models are instantaneous LSTs recorded at a fixed time of a day (about 01:30 pm). Thus, the derived ACPs are not the real values of the annual mean LST, amplitude, and phase. A possible solution is to use the daily mean LST in the YYCD models. However, currently, few studies have reported on the estimations of daily mean LST. Therefore, the development of algorithms for calculating the daily mean LST from the satellite instantaneous observations could contribute to ATC modeling. Moreover, the overpass times of Aqua satellite in the afternoon range from ∼00:30 pm to ∼02:30 pm, and the view angles vary from −55° to 55° [41]; this may introduce some uncertainty to the YYCD models. Thus, the process of temporal or angular normalization of MODIS LSTs may help to improve the accuracy of the YYCD model [42].

Second, the LSTs used in the YYCD models represent clear-sky conditions; this may introduce uncertainties in the ACPs. When the surface is covered by clouds, the thermal infrared sensor (i.e. MODIS) will not be able to calculate the LSTs. The different cloud cover conditions in different regions and seasons will make the annual distribution of LSTs different. The accuracy of the retrieved ACPs should be widely validated with respect to the ground measurements in the near future. Furthermore, the errors in the LSTs caused by the surface covered by partial clouds will increase. One possible solution is to combine the LSTs from the microwave data to fill the gaps formed owing to cloud coverage [43].

V. CONCLUSION

The ATC models are useful tools in modeling the seasonal variation of LSTs. By considering the physical continuity and derivability of the LST variations over several years, the ACP3 and ACP5 models were used in the YYCD models to model year-to-year LST cycles. The examination of global Aqua/MODIS daytime LSTs from 2014 to 2018 showed that the YYCD_ACP3 model achieved a good performance in fitting the time-series LSTs with overall NRMSE of 0.21, R^2 of 0.74, and d of 0.85. The fitting results of ten representative samples show that, except for the two sites located in tropical and South Polar, the YYCD_ACP3 model can obtain a good fitting accuracy with R^2 greater than 0.6. However, the YYCD_ACP5 model with more free parameters can improve the fitting accuracy of the two sites located in the tropical and Antarctic, respectively. Compared with the ACP3 model, which fits the inter-annual LSTs of each year separately, the YYCD_ACP3 model shows a similar performance. However, the fitting curve of the YYCD_ACP3 model is continuous and smooth for the modeling of the inter-annual variation of LST. When fitting the LST variation from 2014 to 2018 as a whole, the YYCD_ACP3 model shows a slightly better performance than the ACP3 model at the ten sites in terms of the NRMSE and R^2. The YYCD_ACP3 model can reflect the variation of LST for each year, while the ACP3 model can only reflect an average variation of LST in these five years. In addition, the YYCD_ACP3 model was applied to reveal the inter-annual variation trend of global LST with MODIS daytime LSTs from 2003 to 2018. Therefore, we recommend using the YYCD models to fit the variations of LST for multiple-years.

ACKNOWLEDGMENT

The authors would like to thank the MODIS Science teams at NASA for providing the satellite observation data.

REFERENCES

[1] M. Anderson, J. Norman, W. Kustas, R. Houborg, P. Starks, and N. Agam, "A thermal-based remote sensing technique for routine mapping of land-surface carbon, water and energy fluxes from field to regional scales," *Remote Sens. Environ.*, vol. 112, no. 12, pp. 4227–4241, Dec. 2008.

[2] Z.-L. Li, B.-H. Tang, H. Wu, H. Ren, G. Yan, Z. Wan, I. F. Trigo, and J. A. Sobrino, "Satellite-derived land surface temperature: Current status and perspectives," *Remote Sens. Environ.*, vol. 131, pp. 14–37, Apr. 2013.

[3] Q. Weng, "Thermal infrared remote sensing for urban climate and environmental studies: Methods, applications, and trends," *ISPRS J. Photogramm. Remote Sens.*, vol. 64, no. 4, pp. 335–344, Jul. 2009.

[4] J. Hansen, M. Sato, and R. Ruedy, "Long-term changes of the diurnal temperature cycle: Implications about mechanisms of global climate change," *Atmos. Res.*, vol. 37, nos. 1–3, pp. 175–209, Jul. 1995.

[5] C. Huang, X. Li, and L. Lu, "Retrieving soil temperature profile by assimilating MODIS LST products with ensemble Kalman filter," *Remote Sens. Environ.*, vol. 112, no. 4, pp. 1320–1336, Apr. 2008.

[6] Y. Li, M. Zhao, S. Motesharrei, Q. Mu, E. Kalnay, and S. Li, "Local cooling and warming effects of forests based on satellite observations," *Nature Commun.*, vol. 6, no. 1, p. 6603, May 2015.

[7] Q. Weng, D. Lu, and J. Schubring, "Estimation of land surface temperature–vegetation abundance relationship for urban heat island studies," *Remote Sens. Environ.*, vol. 89, no. 4, pp. 467–483, Feb. 2004.

[8] B. Bechtel, "Multitemporal landsat data for urban heat island assessment and classification of local climate zones," in *Proc. Joint Urban Remote Sens. Event*, Apr. 2011, pp. 129–132.

[9] F.-M. Göttsche and F. S. Olesen, "Modelling of diurnal cycles of brightness temperature extracted from METEOSAT data," *Remote Sens. Environ.*, vol. 76, no. 3, pp. 337–348, Jun. 2001.

[10] C. Wallace and T. Osborn, "Recent and future modulation of the annual cycle," *Climate Res.*, vol. 22, no. 1, pp. 1–11, 2002.

[11] S.-B. Duan, Z.-L. Li, H. Wu, B.-H. Tang, X. Jiang, and G. Zhou, "Modeling of Day-to-Day temporal progression of clear-sky land surface temperature," *IEEE Geosci. Remote Sens. Lett.*, vol. 10, no. 5, pp. 1050–1054, Sep. 2013.

[12] B. Bechtel, "A new global climatology of annual land surface temperature," *Remote Sens.*, vol. 7, no. 3, pp. 2850–2870, Mar. 2015.
[13] P. Sismanidis, B. Bechtel, I. Keramitsoglou, and C. T. Kiranoudis, "Mapping the spatiotemporal dynamics of Europe's land surface temperatures," *IEEE Geosci. Remote Sens. Lett.*, vol. 15, no. 2, pp. 202–206, Feb. 2018.
[14] P. Fu and Q. Weng, "Variability in annual temperature cycle in the urban areas of the united states as revealed by MODIS imagery," *ISPRS J. Photogramm. Remote Sens.*, vol. 146, pp. 65–73, Dec. 2018.
[15] F. Huang, W. Zhan, J. Voogt, L. Hu, Z. Wang, J. Quan, W. Ju, and Z. Guo, "Temporal upscaling of surface urban heat island by incorporating an annual temperature cycle model: A tale of two cities," *Remote Sens. Environ.*, vol. 186, pp. 1–12, Dec. 2016.
[16] Q. Weng and P. Fu, "Modeling annual parameters of clear-sky land surface temperature variations and evaluating the impact of cloud cover using time series of landsat TIR data," *Remote Sens. Environ.*, vol. 140, pp. 267–278, Jan. 2014.
[17] A. R. Stine, P. Huybers, and I. Y. Fung, "Changes in the phase of the annual cycle of surface temperature," *Nature*, vol. 457, no. 7228, pp. 435–440, Jan. 2009.
[18] M. E. Mann and J. Park, "Greenhouse warming and changes in the seasonal cycle of temperature: Model versus observations," *Geophys. Res. Lett.*, vol. 23, no. 10, pp. 1111–1114, May 1996.
[19] D. J. Thomson, "The seasons, global temperature, and precession," *Science*, vol. 268, no. 5207, pp. 59–68, Apr. 1995.
[20] P. Sismanidis, I. Keramitsoglou, B. Bechtel, and C. Kiranoudis, "Improving the downscaling of diurnal land surface temperatures using the annual cycle parameters as disaggregation kernels," *Remote Sens.*, vol. 9, no. 1, p. 23, Jan. 2017.
[21] W. Zhan, F. Huang, J. Quan, X. Zhu, L. Gao, J. Zhou, and W. Ju, "Disaggregation of remotely sensed land surface temperature: A new dynamic methodology," *J. Geophys. Res., Atmos.*, vol. 121, no. 18, pp. 10538–10554, 2016.
[22] K. Liu, S. Wang, X. Li, and T. Wu, "Spatially disaggregating satellite land surface temperature with a nonlinear model across agricultural areas," *J. Geophys. Res., Biogeosci.*, vol. 124, no. 11, pp. 3232–3251, Nov. 2019.
[23] H. Wu and W. Li, "Downscaling land surface temperatures using a random forest regression model with multitype predictor variables," *IEEE Access*, vol. 7, pp. 21904–21916, 2019.
[24] Y. Xu and Y. Shen, "Reconstruction of the land surface temperature time series using harmonic analysis," *Comput. Geosci.*, vol. 61, pp. 126–132, Dec. 2013.
[25] B. Bechtel and P. Sismanidis, "Time series analysis of moderate resolution land surface temperatures," in *Remote Sensing Time Series Image Processing*. Boca Raton, FL, USA: CRC Press, 2018, pp. 111–142.
[26] B. Bechtel and C. Daneke, "Classification of local climate zones based on multiple earth observation data," *IEEE J. Sel. Topics Appl. Earth Observ. Remote Sens.*, vol. 5, no. 4, pp. 1191–1202, Aug. 2012.
[27] Z. Liu, W. Zhan, J. Lai, F. Hong, J. Quan, B. Bechtel, F. Huang, and Z. Zou, "Balancing prediction accuracy and generalization ability: A hybrid framework for modelling the annual dynamics of satellite-derived land surface temperatures," *ISPRS J. Photogramm. Remote Sens.*, vol. 151, pp. 189–206, May 2019.
[28] Z. Zou, W. Zhan, Z. Liu, B. Bechtel, L. Gao, F. Hong, F. Huang, and J. Lai, "Enhanced modeling of annual temperature cycles with temporally discrete remotely sensed thermal observations," *Remote Sens.*, vol. 10, no. 4, p. 650, Apr. 2018.
[29] P. Fu and Q. Weng, "Temporal dynamics of land surface temperature from landsat TIR time series images," *IEEE Geosci. Remote Sens. Lett.*, vol. 12, no. 10, pp. 2175–2179, Oct. 2015.
[30] J. Quan, W. Zhan, Y. Chen, M. Wang, and J. Wang, "Time series decomposition of remotely sensed land surface temperature and investigation of trends and seasonal variations in surface urban heat islands," *J. Geophys. Res., Atmos.*, vol. 121, no. 6, pp. 2638–2657, Mar. 2016.
[31] M. C. Seiler and F. A. Seiler, "Numerical recipes in C: The art of scientific computing," *Risk Anal.*, vol. 9, no. 3, pp. 415–416, 1989.
[32] C. J. Willmott, S. M. Robeson, and K. Matsuura, "A refined index of model performance," *Int. J. Climatol.*, vol. 32, no. 13, pp. 2088–2094, Nov. 2012.
[33] Z. Wan and Z.-L. Li, "A physics-based algorithm for retrieving land-surface emissivity and temperature from EOS/MODIS data," *IEEE Trans. Geosci. Remote Sens.*, vol. 35, no. 4, pp. 980–996, Jul. 1997.
[34] R. O. Gilbert, *Statistical Methods for Environmental Pollution Monitoring*. Hoboken, NJ, USA: Wiley, 1987.
[35] M. Kendall, *Rank Correlation Methods*, 4th ed, vol. 8. San Francisco, CA, USA: Griffin, 1975.
[36] X. Li, C. Zhang, B. Zhang, and K. Liu, "A comparative time series analysis and modeling of aerosols in the contiguous united states and China," *Sci. Total Environ.*, vol. 690, pp. 799–811, Nov. 2019.
[37] H. B. Mann, "Nonparametric tests against trend," *Econometrica, J. Econ. Soc.*, vol. 13, no. 3, pp. 245–259, 1945.
[38] J. Houghton, *Global Warming: The Complete Briefing*. Cambridge, U.K.: Cambridge Univ. Press, 2009.
[39] R. B. Francini-Filho, R. L. Moura, F. L. Thompson, R. M. Reis, L. Kaufman, R. K. P. Kikuchi, and Z. M. A. N. Leão, "Diseases leading to accelerated decline of reef corals in the largest South Atlantic reef complex (Abrolhos bank, Eastern Brazil)," *Mar. Pollut. Bull.*, vol. 56, no. 5, pp. 1008–1014, May 2008.
[40] G. M. MacDonald, K. V. Kremenetski, and D. W. Beilman, "Climate change and the northern Russian treeline zone," *Phil. Trans. Roy. Soc. B, Biol. Sci.*, vol. 363, no. 1501, pp. 2283–2299, Jul. 2008.
[41] Z. Wan, Y. Zhang, Q. Zhang, and Z.-L. Li, "Validation of the land-surface temperature products retrieved from terra moderate resolution imaging spectroradiometer data," *Remote Sens. Environ.*, vol. 83, nos. 1–2, pp. 163–180, Nov. 2002.
[42] S.-B. Duan, Z.-L. Li, B.-H. Tang, H. Wu, and R. Tang, "Generation of a time-consistent land surface temperature product from MODIS data," *Remote Sens. Environ.*, vol. 140, pp. 339–349, Jan. 2014.
[43] S.-B. Duan, Z.-L. Li, and P. Leng, "A framework for the retrieval of all-weather land surface temperature at a high spatial resolution from polar-orbiting thermal infrared and passive microwave data," *Remote Sens. Environ.*, vol. 195, pp. 107–117, Jun. 2017.

ZEFENG XING received the B.E. degree in remote sensing of technology from the Heilongjiang Institute of Technology, Heilongjiang, China, in 2013, and the M.S. degree in cartography and geographic information system from the University of Chinese Academy of Sciences, Beijing, China, in 2016. He is currently pursuing the Ph.D. degree in agricultural remote sensing with the Key Laboratory of Agricultural Remote Sensing, Ministry of Agriculture/Institute of Agricultural Resources and Regional Planning, Chinese Academy of Agricultural Sciences, Beijing, China.

YANRU YU received the B.S. degree in management and the M.S. degree in geological engineering from Hebei GEO University, Hebei, China, in 2014 and 2018, respectively. She is currently pursuing the Ph.D. degree with the Institute of Agricultural Resources and Regional Planning, Chinese Academy of Agricultural Sciences, Beijing, China, in 2018. Her research interest includes agricultural quantitative remote sensing.

SI-BO DUAN (Member, IEEE) received the Ph.D. degree in cartography and geographical information system from the Institute of Geographic Sciences and Natural Resources Research, Chinese Academy of Sciences, Beijing, China, in 2014. He is currently an Associate Professor with the Key Laboratory of Agricultural Remote Sensing, Ministry of Agriculture and Rural Affairs/Institute of Agricultural Resources and Regional Planning, Chinese Academy of Agricultural Sciences, Beijing. His research interest includes the retrieval and validation of land surface temperature.

ZHAO-LIANG LI received the B.A. degree in photogrammetry from the Wuhan Technical University of Surveying and Mapping, China, in 1985, and the M.S. degree in imaging processing and computer graphics and the Ph.D. degree in terrestrial environmental physics from the University of Louis Pasteur, Strasbourg, France, in 1987 and 1990, respectively.

Since 1992, he has been a Research Scientist with CNRS, Illkirch, France. He joined the Institute of Agricultural Resources and Regional Planning, Chinese Academy of Agricultural Sciences, in 2013. He has participated in many national and international projects, such as the National Aeronautics and Space Administration (NASA)-funded Moderate Resolution Imaging Spectroradiometer, European Community (EC)-funded program Exploitation of angular effects in land surface observations from satellites (EAGLE), and ESA-funded programs SPECTRA. He has authored more than 200 articles in international refereed journals. His main research interests include thermal infrared radiometry, parameterization of land surface processes at large scale, and assimilation of satellite data to land surface models.

MAOFANG GAO (Member, IEEE) received the Ph.D. degree in agricultural remote sensing from the Chinese Academy of Agricultural Sciences, Beijing, China, in 2011.

She is currently an Associate Professor with the Key Laboratory of Agricultural Remote Sensing, Ministry of Agriculture and Rural Affairs/Institute of Agricultural Resources and Regional Planning, Chinese Academy of Agricultural Sciences. Her research interests include agricultural remote sensing and simulation of carbon–nitrogen cycle.

PEI LENG received the Ph.D. degree in cartography and geographical information system from the University of Chinese Academy of Sciences, Beijing, China, in 2015.

He is currently an Associate Professor with the Key Laboratory of Agricultural Remote Sensing, Ministry of Agriculture and Rural Affairs/Institute of Agricultural Resources and Regional Planning, Chinese Academy of Agricultural Sciences, Beijing. His research interests include the methodological developments of satellite soil moisture and energy fluxes retrievals, and the determination of agricultural water consumption and irrigation water from remote sensing data.

XIA ZHANG was born in Shijiazhuang, Hebei, China, in 1985. She received the B.S. degree in geographic information system from Changchun Normal University, Changchun, China, in 2008, and the M.S. and Ph.D. degrees in cartography and geographic information system from Northeast Normal University, Changchun, in 2010 and 2014, respectively.

Since 2014, she has been a Lecturer with the College of Land Resources and Urban and Rural Planning, Hebei GEO University, Shijiazhuang. Her research interests include the thermal infrared (TIR) polarization remote sensing, multiangle and hyperspectral remote sensing, and quantitative remote sensing.

GUOFEI SHANG was born in Tangshan, Hebei, China, in 1964. He received the B.E. degree in aerial photogrammetry and remote sensing from Wuhan University, Wuhan, China, in 1985, and the M.E. and Ph.D. degrees in land resources management from the Renmin University of China, Beijing, China, in 1992 and 2002, respectively.

Since 1997, he has been a Professor and the Dean of the College of Land Resources and Urban and Rural Planning, Hebei GEO University, Shijiazhuang, China. His research interests include aerial photogrammetry and remote sensing, quantitative remote sensing, and natural resources management.